



Bulletin of the Mineral Research and Exploration

<http://bulletin.mta.gov.tr>



Magnetic anomalies and geological signatures in the Black Sea: a comprehensive study of the east and west basins

İlkin ÖZSÖZ^{a*}, Eşref AYLAN^a and Ceyhan Ertan TOKER^a

^a General Directorate of Mineral Research and Exploration, Marine Research Department, Ankara, Türkiye

Research Article

Keywords:

Curie Point Depth, Heat Flow, Tilt Derivative, Local Wavenumber, Correlation Plot.

ABSTRACT

This study investigates the origin of the Black Sea, focusing on the East and West Black Sea basins. Data such as Curie Point Depth values, heat flow, bathymetry, Moho depth, sediment thickness, and magnetic depth estimation were analyzed to explore the region's geological features. Correlations between these parameters were assessed for each basin, shedding light on their tectonic history and the influence of volcanic rocks. Thinner sedimentary covers enhanced the detectability of rocks with higher magnetic properties, while the interiors showed lower magnetic anomalies due to younger sedimentary rocks. Edge detection techniques, like tilt angle and Local Wavenumber methods, improved magnetic data interpretation. The study computed Curie Point Depth and heat flow using 65 blocks, revealing greater depths in the Western Black Sea (up to 32 km) compared to the Eastern Black Sea (24-28 km). Two profiles (A-A' and B-B') were examined for further insights. Overall, this study provides valuable insights into the geological evolution of the Black Sea basins.

Received Date: 23.05.2024

Accepted Date: 04.03.2025

1. Introduction

To limit the thermal structure and lithospheric rheology, it is significant to assess the spatial discrepancies in temperature across the Earth (Audet and Gosselin, 2019; Sobh et al., 2021). In addition, analysing the variances in magnetic data and the depth of the Moho can provide insight into the tectonic evolution of the region. Calculating the depth of the Curie point, at which crustal rocks reach their Curie temperature [approximately 580° for magnetite (Dunlop et al., 1998)], provides temperature constraints over a region. When rocks are heated above the Curie temperature, they lose their ferromagnetic magnetism and become paramagnetic. Thus, the depth of the magnetised crust can be determined by identifying the

Curie depth, which is the point at which rocks lose their ability to preserve ferromagnetic magnetism (Haggerty, 1978).

Although estimating the Curie depth from magnetic data is significant, uncertainties remain as to whether spectral techniques can produce dependable depth estimates and whether these estimations portray the Curie isotherms or a structural boundary. To clarify this issue, optimum wavenumber ranges for estimating Curie depth was limited by comparing theoretical approximation and linear estimation (Núñez Demarco et al., 2021; Pamuk and Özsöz, 2022). Furthermore, additional constraints such as uncertainties in Curie depth estimation, Moho depth, sediment thickness, and magnetic depth estimation techniques can be

Citation Info: Özsöz, İ., Aylan, E., Toker, C. E. 2025. Magnetic anomalies and geological signatures in the Black Sea: a comprehensive study of the east and west basins. Bulletin of the Mineral Research and Exploration 176, 115-133. <https://doi.org/10.19111/bulletinofmre.1651250>

*Corresponding author: İlkin ÖZSÖZ, ilkin.ozsoz@mta.gov.tr

employed to verify the estimations of Curie depth (Özsöz, 2021).

Numerous researchers have conducted studies on the thermal composition of the Black Sea's crust, specifically within the West and East Black Sea Basins (WBS and EBS). Maden (2013) investigated the EBS and determined that the elevated values of heat flow observed may be attributed to the melting of the lithospheric mantle, triggered by the upwelling of the asthenosphere. Starostenko et al. (2014) noted that the WBS and EBS exhibit a greater depth for the Curie point (CPD) as compared to the Mid-Black Sea Ridge (MBSR) and coastal regions, which are characterised by thinner sediment layers. This finding suggests that areas with thicker sediment deposits correspond to deeper CPD values. In their study, Tütünsatar et al. (2018) presented findings on the fluctuating heat flow values in the Black Sea, ranging from 22 mW/m² to 41 mW/m². They posited that regions with higher heat flow values than the average are indicative of potential deep fault zones and areas where gas migration occurs. Entezar-Saadat et al. (2020) presented a comprehensive lithospheric model of the Black Sea, incorporating thermal structure, sediment thickness, and the depths to the Moho and lithosphere-asthenosphere boundary (LAB). The study utilized a combination of 3D nonlinear inversion of satellite gravity and gravity gradiometry data with 2D iterative forward modelling of potential field data and heat flow measurements. The findings revealed that the average basement depths are 10–11 km in the East Black Sea (EBS) and 11–12 km in the West Black Sea (WBS), with shallower depths of 2–5 km beneath ridges. The mean crustal thickness was determined to be 20 km in the EBS and 21 km in the WBS. Additionally, the surface heat flow was found to be highest on the ridges and lowest over the thick central sedimentary basins. This model offers a detailed and integrated understanding of the Black Sea's lithospheric structure. Bilim et al. (2021) shed light on crustal thickness beneath the Black Sea and surrounding region by gravity data. Their findings indicate that the Shatsky Ridge displays the thinnest crustal thickness at 10 km, while the Sea of Azov boasts the greatest crustal thickness, measuring at 28 km. Akar (2024) conducted a study in the Çameli Basin and its surrounding region in southwestern

Anatolia, Türkiye, utilizing aeromagnetic data and a fractal-based centroid method to estimate the Curie Point Depth, which is essential for understanding regional tectonic and geothermal characteristics. The estimated depths of magnetic sources range between 6.9 and 14.05 km, while the thermal gradient varies from 41.28°C/km to 89.23°C/km, with an average value of 58.59°C/km. The results correspond with NW-SE earthquake distributions and indicate that the Curie isotherm is significantly shallower than the Moho boundary.

The primary objective of this study is to establish a comprehensive theoretical framework elucidating the origin and evolution of the Black Sea, with a specific focus on both the EBS and WBS basins. To achieve this, a wide array of data is employed, encompassing parameters such as CPD (Curie Point Depth) values, heat flow values derived from CPD data, bathymetry, Moho depth, sediment thickness, and magnetic depth estimation techniques (Tilt depth and Local Wavenumber methods). The investigation also examines how the distribution of volcanic rocks in the Black Sea region impacts magnetic anomalies. Furthermore, a meticulous analysis of the correlation between CPD values, bathymetry, Moho depth, sediment thickness, tilt depth, and Local Wavenumber depths is conducted separately for the EBS and WBS basins. By closely examining these correlations and considering the tectonic history and presence of volcanic rocks, the notable discrepancies between the EBS and WBS are thoroughly interpreted. This research aims to shed light on the distinct geological processes and factors that have contributed to the development and divergence of the EBS and WBS basins.

2. Geological Setting

The Black Sea, a large semi-enclosed basin, is surrounded by orogenic belts in the south (Pontides), northeast (Crimea Mountains and Greater Caucasus), and west (Balkanides). Beneath the Neogene to present-day sedimentary succession of the basin fill, representing a unified depocenter, lie two sub-basins, namely the WBS and the EBS, along with a structural high, the Mid Black Sea Ridge (MBSR), comprising Andrusov Ridge and Arkhangelsky Ridge in an

en-echelon arrangement. The WBS and EBS display distinct differences in structural complexity, with the latter featuring a prominent ridge (Shatsky) and a pair of troughs (Tuapse and Sorokin) near its northeastern margin.

The Black Sea Basin is categorized as a back-arc basin, resulting from the northward subduction of the Neo-Tethys Ocean under the southern margin of Laurasia (Letouzey et al., 1977; Zonenshain and Le Pichon, 1986; Finetti et al., 1988). The process of rifting in the extensional back-arc led to the separation of a continental fragment (İstanbul Zone) from the Moesian Platform, giving rise to the asymmetric WBS, where the southern margin exhibits a steeper inclination (Okay et al., 1994; Nikishin et al., 2015). On the other hand, the EBS took shape through the separation and rotation (Okay et al., 1994; Robinson et al., 1996) of the Mid MBSR from the Shatsky Ridge, forming a more symmetrical basin (Shillington et al., 2009). The timing of sub-basin formation is generally believed to be late Cretaceous to early Paleogene, with the EBS considered to be the younger of the two, a subject of ongoing debate (Görür, 1988; Görür et al., 1993; Robinson et al., 1995; Okay and Şahintürk, 1997; Hippolyte et al., 2017; 2018).

The two sub-basins are situated on crusts with distinct thermal and mechanical properties (Spadini et al., 1996). After the initial rifting, the WBS evolved into a proper ocean with an inferred oceanic crust, likely during the late Santonian period, indicated by the age of corresponding pelagic sediments and volcanics in the Pontides region (Tüysüz et al., 2012; Tüysüz, 2018). On the other hand, the EBS has a thinned continental or an oceanic crust beneath it (Shillington et al., 2009), and its opening started in the late Paleocene and was completed in the middle Eocene (Robinson et al., 1995). The sedimentary fill thickness in the WBS ranges from 14 to 18 km, whereas in the EBS, it can reach up to 12 km.

Seismic surveys have revealed the presence of multiple buried volcanoes along the southern offshore margin of the Black Sea basin and on the Shatsky and Andrusov ridges (Nikishin et al., 2015). Due to the absence of sufficient well data, the age of these volcanoes is inferred to be likely Santonian-

Campanian based on the correlation with volcanic units in the Pontides and Crimea regions (Nikishin et al., 2003).

Based on seismic reflection studies (Letouzey et al., 1977; Nikishin et al., 2015), the undisturbed post-rift sedimentary layers within the basin indicate that the crust beneath the Black Sea basin possesses sufficient strength to withstand the tectonic forces responsible for the deformation of its margins since at least the Eocene period (Espurt et al., 2014). GPS measurements (Tari et al., 2000) and seismic activity (Neprochnov and Ross, 1978) indicate an active shortening on the EBS. Figure 1 illustrates simplified tectonic map of the study area.

3. Data

The magnetic data used in this study was obtained from the EMAG 2 model. The EMAG 2 model presents a detailed description of the Earth's magnetic field on a global scale. It was calculated using satellite magnetic data as well as land and sea measurements. The EMAG 2 model can identify magnetic anomalies larger than 1 nT with a coverage of 2 arc-minutes and a spatial resolution of approximately 4 km. (Maus et al., 2009).

A robust inversion approach that has been widely validated in multiple regional studies is used to extract the first global model of Curie-point depth (GCDM) from magnetic anomaly inversion based on fractal magnetisation (Li et al., 2017). According to the statistical analysis, the mean depth of the Curie point in the marine zone is lower than in the continental region. The continental Curie depths, on the other hand, have a virtually bimodal distribution, with some old cratons having shallow Curie points. Hydrothermal circulations in young oceanic lithosphere and thermal disturbances in old oceanic lithosphere affect oceanic Curie depths. Furthermore, the oceanic Curie depths are heavily dependent on the spreading rate along active spreading centres (Li et al., 2017). In this research, the estimated Curie-depth points were compared and validated with the global model of Curie-point depth within the same geographical region.

The bathymetry data used in this study, which focused on the Black Sea region, was obtained

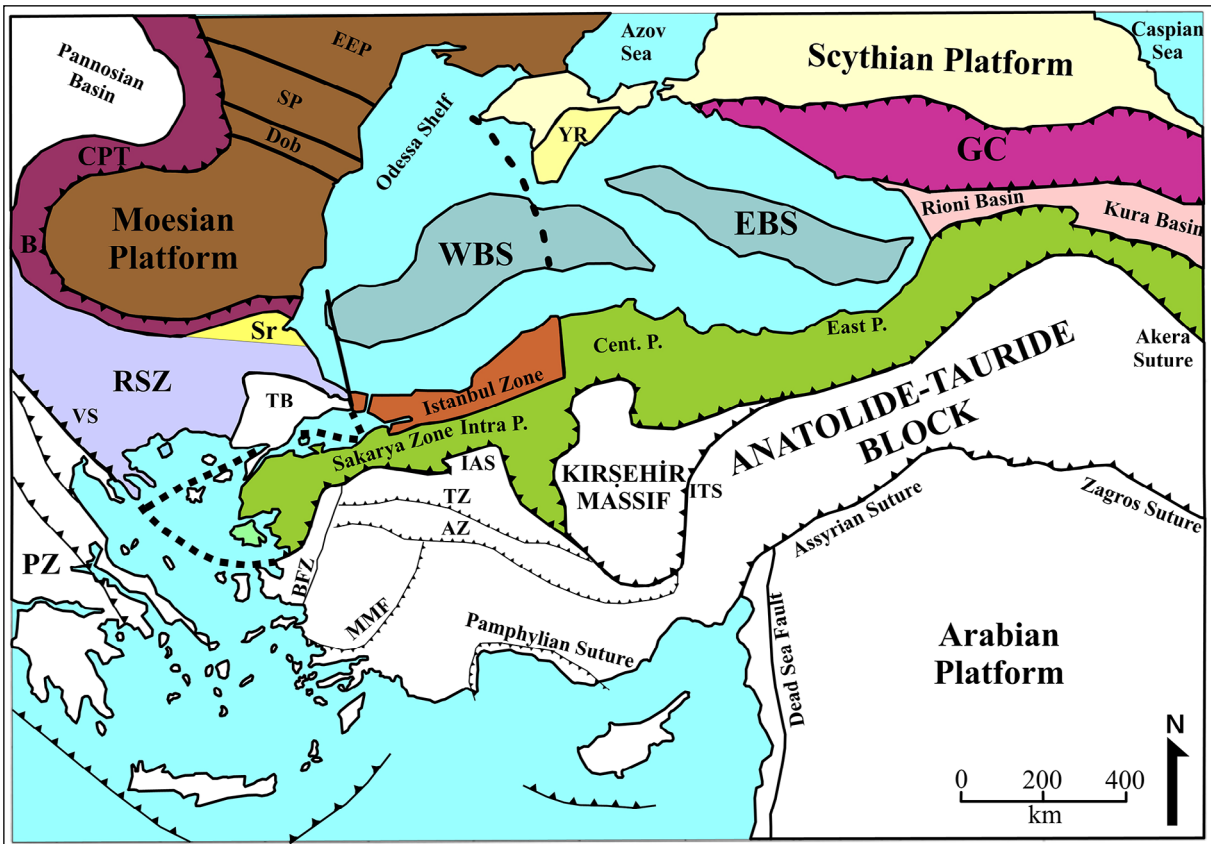


Figure 1- Simplified tectonic map of the Black Sea and its surrounding regions (modified after Şengör, 1984; Okay, 1989; Okay and Tüysüz, 1999; Özsöz and Tokar, 2022). PZ= Pelagonian Zone, VS= Vardar Suture, RSZ= Rhodope-Strandja Zone, B= Balkanides, CPT= Carpathians, Dob= Dobruđja, SP= Scythian Platform, EEP= East European Platform, YR= Yayla Range, WBS=West Black Sea Basin, EBS= East Black Sea Basin, GC= Greater Caucasus, Intra P.= Intra Pontide Suture, Cent. P.= Central Pontides, East P.= Eastern Pontides, IAS= İzmir - Ankara Suture, TZ= Tavşanlı Zone, AZ= Afyon Zone, MMF= Menderes Massif, BFZ= Bornove Flysch Zone, SR= Srednogie).

from the ETOPO 1 model. ETOPO 1 model includes combination of land topography and ocean bathymetry into a global grid. The model was developed by The National Oceanic and Atmospheric Administration (NOAA). ETOPO1 grid cell spans an area of around 1.8 km² at a resolution of one arc-minute at the equator. The model is constructed with an integration of satellite and marine observations, as well as data from other sources. ETOPO1 is widely used in oceanography, geology, and climate research because it provides a precise depiction of the Earth's topography, including mountain ranges, valleys, and oceanic trenches (Amante and Eakins, 2009).

Moho depth and sediment thickness data were obtained from CRUST1.0 model. CRUST1.0, 1-by-1° global crustal model, which forms the initial framework for the comprehensive database to compile

a worldwide model of the Earth's crust and lithosphere, LITHO1.0 (Pasyanos et al., 2013). The Moho depth and sediment thickness featured in CRUST1.0 is based on 1-degree averages obtained from a recently updated database of crustal thickness data gathered from active-source seismic studies, as well as from receiver function studies (Laske et al., 2013).

4. Methods

4.1. CPD Estimation

The Curie temperature is the fundamental physical phenomenon that controls the exploration of magnetic depth method. This method's ability to detect magnetic bodies is restricted by the depth of the Curie isotherm. It is feasible to utilize magnetic data to deduce heat flow since the magnetic characteristics of rocks are dependent by temperature,

and rocks lose their magnetic properties at the Curie temperature. Nonetheless, this methodology is subject to certain limitations due to its dependence on several assumptions. The technique requires that the magnetic sources' depth be significantly greater than their height, which is vital for spectral separation (Bouguern et al., 2015).

The estimation of CPDs has been accomplished in numerous locations across the globe through the application of magnetic data. Two primary techniques have been employed to calculate CPDs: the spectral peak and the centroid depths. The spectral peak method was initially introduced by Spector and Grant (1970), while the centroid approach was first presented by Bhattacharyya and Leu (1977) and was later improved by Okubo et al. (1985). In this study, the latter approach was used.

Our assumption is that the lithosphere's magnetised layer is limited by two surfaces situated at depths Z_t (the top of the magnetised layer) and Z_b (the bottom of the magnetised layer). It should be noted that if $Z_t = 0$, this would imply that the magnetised layer's top coincides with the measurement plane (Sobh et al., 2021). The thickness of the magnetised layer is represented by ΔZ , which is equal to Z_b minus Z_t (Figure 2).

Rozimant et al. (2009) identified a correlation between heat flow and Curie Point Depth (CPD) values but noted that this relationship does not consistently align with crustal depth. They also emphasized that the Curie point isotherm marks the boundary between the magnetic and non-magnetic regions of the crust.

Spector and Grant (1970) first introduced the method of radially averaging power spectra, which provides information about the depth of the magnetic layer. Subsequently, this method has been improved upon by Bhattacharyya and Leu (1975), Connard et al. (1983), Okubo et al. (1985), Tanaka et al. (1999), Ross et al. (2006). These advancements enable the thermal structure of an area to be determined using magnetic anomaly values. In simple terms, the radially averaged spectrum can be defined as:

$$P(|k|) = Ae^{-2|k|z_t}(1 - e^{-|k|(z_b-z_t)})^2 \tag{1}$$

where A is constant, wavenumber represented by k, and depth measurements for the top and bottom of a magnetic source, denoted as Z_b and Z_t . The next step in the equation 1 involves taking the natural logarithm of both sides.

$$\ln[P(|k|)] = \ln[A] - 2Z_t(k) + 2\ln [1 - e^{-|k|(z_b-z_t)}] \tag{2}$$

When the wavenumber components are of high or medium values, the exponential factor in equation

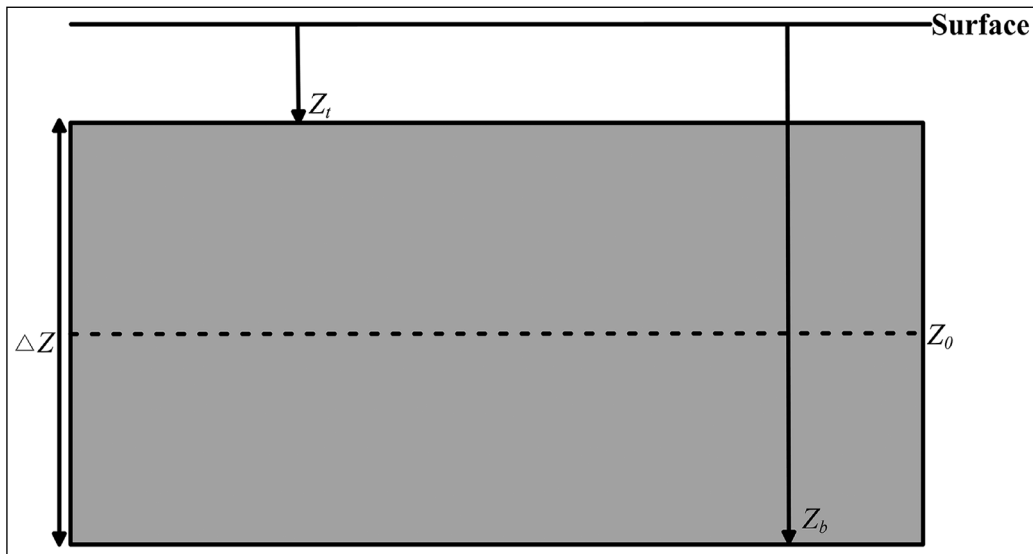


Figure 2- Schematic diagram of magnetic depths where Z_t = top of the magnetised layer, Z_b = the bottom of the magnetised layer, Z_0 = centroid depth that corresponds to $\frac{Z_b+Z_t}{2}$ and ΔZ = thickness of the magnetised layer.

2 becomes insignificant and can be disregarded. As a result, equation 2 can be expressed differently as shown in the following rewritten form:

$$\ln[P(|k|)] = \ln[A] - |k|2Z_t \quad (3)$$

Equation 3 indicates that the slope is equal to $2Z_t$. By dividing equation 3 by 2, a linear estimation model can be derived:

$$\ln[P(|k|)^{1/2}] = C - |k|Z_t \quad (4)$$

The equation 4 involves a constant value, denoted as C. The slope of equation 4 is indicative of the depth measurement to the top of the magnetic layer, represented as Z_t . To obtain an estimation for Z_0 , one can multiply equation 1 by $e^{-|k|(z_0-z_0)}$, and then divide the resulting equation by 2:

$$\ln[P(|k|)^{1/2}] = Ae^{-|k|z_0}(e^{-|k|(z_t-z_0)} - e^{-|k|(z_b-z_0)}) \quad (5)$$

The depth to the centroid of the magnetic source is denoted by Z_0 . If we substitute the first terms of the Taylor series expansion for the exponential term in equation 5, an approximate equation for Z_0 can be obtained.

$$\ln[P(|k|)^{1/2}] \approx Ae^{-|k|z_0}(Z_b - Z_t) \quad (6)$$

The thickness of the magnetic crust (ΔZ) is represented by $Z_b - Z_t$, as defined by Gasparini et al. (1979). By substituting and rearranging the thickness of the magnetic crust with Z_0 , we obtain:

$$\ln \left[\frac{P(|k|)^{1/2}}{|k|} \right] = \ln[C_2] - |k|Z_0 \quad (7)$$

Equation 7 involves a constant value for C_2 , while Z_0 is determined by calculating the slope for the low wavenumber components. The depth of the magnetic layer's centroid is related to the magnetic layer's bottom, as indicated by Okubo et al., (1985) and Tanaka et al., (1999):

$$Z_b = 2Z_0 - Z_t \quad (8)$$

Overall, equation 4 and 7 represent straight-line equations, and ultimately, the estimation of Z_t and Z_0 can be achieved by determining the slope of the linear fit. Once Z_t and Z_0 are estimated, it is possible to articulate the uncertainty (ΔZ_t and ΔZ_0) associated with these estimations in the following manner (Martos et al., 2017; Carrillo-de la Cruz et al., 2020):

$$\Delta Z_t = (RMS_{Z_t}/2\pi) \times [\max(k_{s_{Z_t}}) - \min(k_{s_{Z_t}})] \quad (9)$$

$$\Delta Z_0 = (RMS_{Z_0}/2\pi) \times [\max(k_{s_{Z_0}}) - \min(k_{s_{Z_0}})] \quad (10)$$

The expressions RMS_{Z_t} and RMS_{Z_0} refer to the Root Mean Square (RMS) error of the linear regression model divided by the number of data points used in the analysis. On the other hand, $k_{s_{Z_t}}$ and $k_{s_{Z_0}}$ represent the wavenumber range of the linear segment chosen to estimate Z_t and Z_0 , respectively. Ultimately, the uncertainty in the estimated value of Z_b denoted as ΔZ_b can be expressed as per the definition proposed by Martos et al. (2019):

$$\Delta Z_b = \sqrt{2\Delta Z_0^2 - \Delta Z_t^2} \quad (11)$$

4.1.1. Wavenumber Ranges for Curie Depth Estimations

To ensure the accuracy of the calculated Z_b and Z_t values, it is essential to validate them by comparing with both theoretical approximations and linear estimations. However, many authors tend to overlook this step and manually select the wavenumber ranges. In a recent study, Núñez Demarco et al. (2021) analyzed 72 articles and recommended that the mathematical validity of the computation can be evaluated by comparing the results of equations (2) and (3) for Z_t and equations (5) and (6) for Z_b . The comparison can be done by examining the difference in the slope between the linear estimation model and the theoretical curve.

$$\Delta m = \left[\frac{t(k_{i+1}) - t(k_i)}{k_{i+1} - k_i} - \frac{l(k_{i+1}) - l(k_i)}{k_{i+1} - k_i} \right] \quad (12)$$

The symbol Δm denotes the difference in slope, where $t(k)$ represents the theoretical curve and $l(k)$ denotes the linear estimation. When Δm approaches 0, it implies that the estimated values of Z_0 and Z_t are reliable. Specifically, wavenumber ranges that exhibit a difference of less than 5% between the linear approximation and the theoretical curve can be considered as valid regions for estimating Z_0 and Z_t . Generally, the valid regions for Z_t are larger than those for Z_0 . As the thickness of the magnetic layer (ΔZ) increases, the valid regions tend to be wider for Z_t and narrower for Z_0 . Additionally, when Z_t is deeper for a constant ΔZ , the confidence region becomes broader.

Figure 3 shows that the regions of confidence are estimated for the expected maximum, minimum, and average values of magnetic thickness (ΔZ). In order to achieve the expected maximum value of ΔZ (34 km),

the maximum expected value of Z_b is taken as 36 km, while the minimum expected value of Z_t is taken as 2 km. Similarly, to obtain the expected average value of ΔZ (23 km), the expected average values of Z_b and

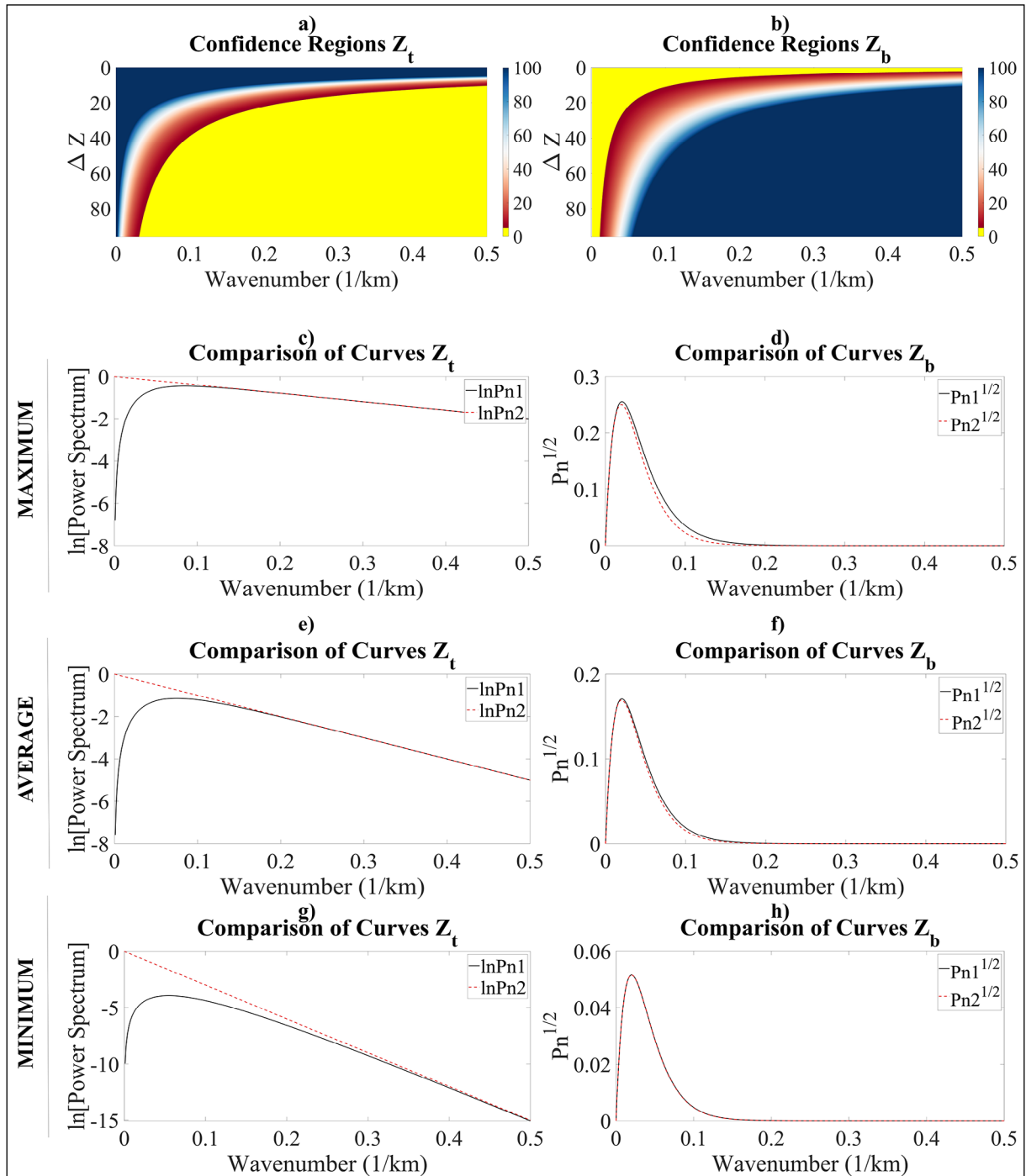


Figure 3- The confidence regions for CPD estimations are presented in the following manner: panels a) and b) display reliable ranges of wavenumbers, represented by the yellow area, where the slope difference (Δm) is less than 5%. Panels c) and d) illustrate the wavenumber ranges associated with the maximum value of ΔZ (34 km), where $Z_b = 36$ km, $Z_t = 2$ km. Panels g) and h) show the wavenumber ranges corresponding to the average value of ΔZ (23 km), where $Z_b = 28$ km, $Z_t = 5$ km. Panels e) and f) depict the wavenumber ranges for the minimum value of ΔZ (7 km), where $Z_b = 22$ km, $Z_t = 15$ km.

Z_t are assumed as 28 km and 5 km, respectively. To achieve the expected minimum value of ΔZ (7 km), the expected minimum values of Z_b and Z_t are taken as 22 km and 15 km, respectively. The assumptions for the expected values of Z_t and Z_b are based on previous studies conducted by Starostenko et al. (2014), Li et al. (2017), Tütünsatar et al. (2018).

4.1.2. Heat Flow Estimations from CPD Results

The estimation of heat flow and thermal gradient is carried out utilizing Fourier's Law (Fourier, 1878). As CPD is connected with magnetite's 580 °C temperature, heat flow can be determined based on the estimated Z_b values. The heat flow can be given as:

$$q(z) = \lambda \frac{dT(z)}{dz} \quad (13)$$

where $q(z)$ is heat flow as a function of depth (z), λ is the thermal conductivity with a value of 2.2 W/mK and $\frac{dT}{dz}$ is the geothermal gradient. To solve equation 13 for conductive heat transfer, which is outlined in (Martos et al., 2017), it is necessary to determine the boundary limits. Thus, the equation can be rearranged and expressed as:

$$q(z) = \lambda \frac{(T_c - T_0)}{Z_b} \quad (14)$$

Equation 10 considers T_c as the Curie temperature of magnetite (approximately 580°C), while T_0 represents the surface temperature, which has a value of 20°C. Notably, the equation 14 does not account for radiogenic heat production, mass advection, temperature dependence of thermal conductivity, and transient cooling, as described in (Ravat et al., 2016).

4.2. Edge Detection and Depth Estimation Methods

4.2.1. Tilt Depth Method

The magnetic tilt angle is a mathematical expression that is normalized by comparing the vertical and horizontal derivatives of the reduction to the pole (RTP) field. This approach is called the "tilt depth method" and enables a more intuitive comprehension of the changes in depth of magnetic source bodies (Salem et al., 2007). Tilt angle is initially introduced by Miller and Singh (1994). The most basic version of the tilt depth method assumes that the source formations have perpendicular interfaces, no remnant magnetism,

and that the magnetisation is oriented vertically. Then the method was subsequently refined by Verduzco et al. (2004), and subsequently defined as:

$$\theta = \arctan \left[\frac{\frac{\partial M}{\partial z}}{\frac{\partial M}{\partial H}} \right] \quad \text{where} \quad \frac{\partial M}{\partial H} = \sqrt{\left(\frac{\partial M}{\partial x} \right)^2 + \left(\frac{\partial M}{\partial y} \right)^2} \quad (15)$$

where $\partial M/\partial x$, $\partial M/\partial y$, and $\partial M/\partial z$ represent the first order differentials of the magnetic field with respect to the x, y, and z axes, correspondingly. Additionally, $\frac{\partial M}{\partial H}$ is total horizontal derivative of the magnetic field M. One can observe several interesting attributes of the tilt angle (θ). Specifically, due to the nature of the "tan⁻¹" trigonometric function, the magnitude of all tilts falls within the range of -90° to +90°, independent of the magnitude of the vertical or absolute value of the overall horizontal gradient. In addition to equalizing the amplitude of magnetic anomalies across a grid or profile, this approach preserves the spectral consistency of the signal, thereby enabling additional quantitative analysis such as the determination of local wavenumber (Salem et al., 2007).

Tilt angle over the edges of the contact is 0° ($h=0$), while it reaches 45° when h equals Z_{tilt} and -45° when h is $-Z_{tilt}$. As a result, it is plausible to use contours of the magnetic tilt angle to determine both the location ($\theta=0^\circ$) and top depth (half the physical distance between $\pm 45^\circ$ contours) of contact-like formations (Doğru et al., 2017). This phenomenon quantitatively identified as (Salem et al., 2007):

$$\theta = \arctan \left(\frac{h}{Z_{tilt}} \right) \quad (16)$$

where h is horizontal distance and Z_{tilt} refers to the depth of the top of contact-like structures that have been estimated through the use of the tilt-depth method.

4.2.2. Local Wavenumber Method

The method of determining the local wavenumber requires the calculation of both first and second derivatives in both horizontal and vertical directions. It is the most vulnerable to disturbances from noise and interference. However, if such disturbances are absent, this method can provide precise measurements of the horizontal and vertical positions of individual sources,

as well as the sources' structural characteristics (Phillips, 2000). According to Thurston and Smith (1997) work, they provide a formula for determining the local wavenumber along a 2-dimensional source by measuring a profile. Subsequently, Phillips (2000) derived an equivalent formula for the local wavenumber (LW) of the anomalous magnetic field in a gridded format:

$$LW = \frac{1}{\left(\frac{\partial M}{\partial x}\right)^2 + \left(\frac{\partial M}{\partial y}\right)^2 + \left(\frac{\partial M}{\partial z}\right)^2} \left[\frac{\partial M}{\partial x} \frac{\partial^2 M}{\partial z \partial x} + \frac{\partial M}{\partial y} \frac{\partial^2 M}{\partial z \partial y} + \frac{\partial M}{\partial y} \frac{\partial^2 M}{\partial z \partial z} \right] \quad (17)$$

The LW technique, which employs the second-order derivatives, is susceptible to noise and aliasing in the data, resulting in frequent occurrence of discontinuous contacts and inadequate management of strike direction.

Depth estimations can be conducted by LW with appropriate structural index (*N*). The numerical value assigned to the structural index differs depending on the geological feature being analysed. A value of zero is assigned to the uppermost portion of a contact or

fault that extends to a significant depth, while a value of one corresponds to the edge of a thin sheet. An extended pipe or cylinder is assigned a value of two, while the centroid of a sphere or dipole is assigned a value of three. The local wavenumber method can accurately determine depths for straightforward sources. However, it fails for thick dikes because of the interfering effects of the two corners, as do all other methods (Phillips, 2000). Depth is estimated using equation 18.

$$\text{At peak} \rightarrow Z_{LW} = \frac{(N + 1)}{LW} \quad (18)$$

where *N* is structural index which is taken as 0 for this study and *Z_{LW}* is estimated depth from local peak of LW grid.

5. Results and Discussion

The magnetic data obtained from the EMAG2 model was subjected to the RTP technique, employing a predetermined declination of 6.87°±0.35° and an inclination of 61.43°±0.21°. In Figure 4, the RTP

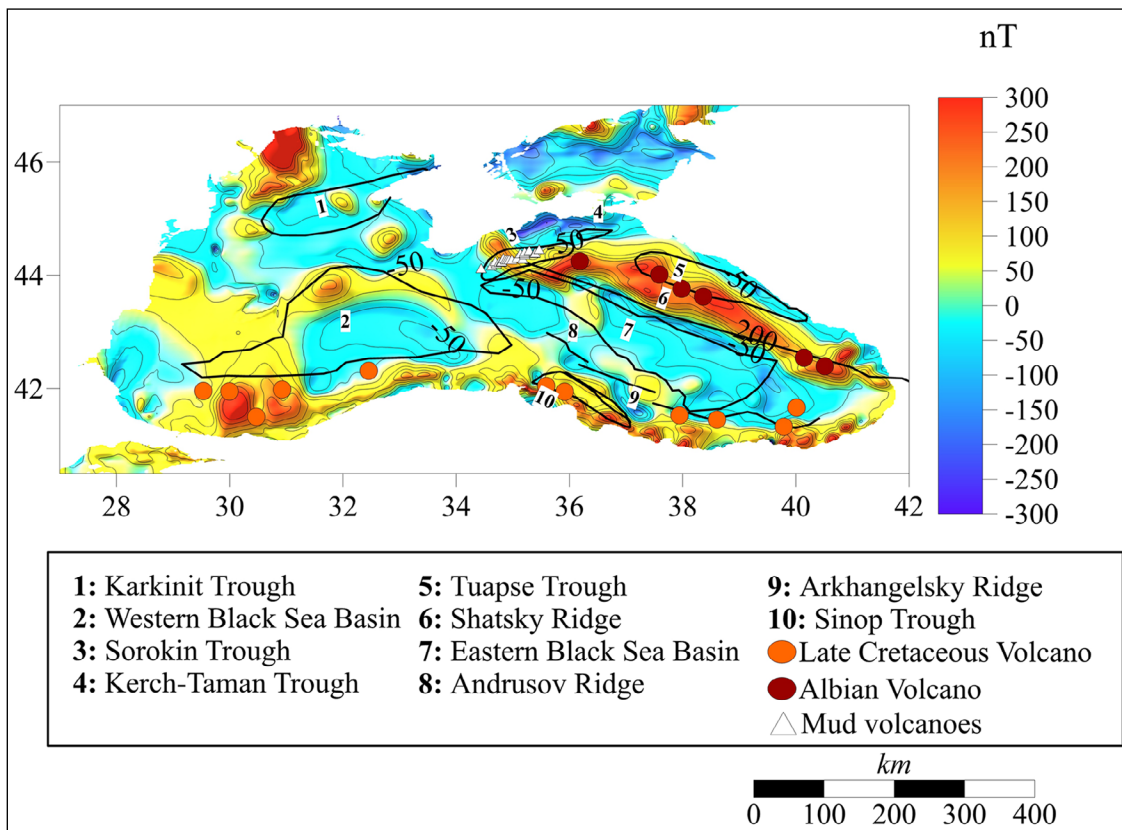


Figure 4- RTP magnetic anomaly with tectonic features in the study area.

magnetic anomaly is depicted, illustrating discernible tectonic features that contribute to the overall magnetic profile.

In each map, the locations of Cretaceous Volcanoes are derived from Nikishin et al. (2015) and Tari and Simmons (2018), while the locations of Albian Volcanoes are sourced from Nikishin et al. (2015). Additionally, the locations of mud volcanoes are digitized based on the data presented in Wagner-Friedrichs et al. (2008).

The range of RTP magnetic anomalies spans from -300 nT to 300 nT, with the most prominent magnetic anomalies localized along the Shatsky Ridge and basin boundaries. Conversely, the EBS and WBS exhibit relatively lower magnetic anomalies. The higher magnetic anomalies observed in the Shatsky Ridge and basin boundaries can be attributed to the prevalence of older magnetic-rich rocks. These regions are predominantly composed of rocks characterized by a high abundance of magnetic minerals, including magnetite, which contribute to the manifestation of larger magnetic anomalies. Additionally, the relatively thinner sedimentary layer in these areas facilitates the detection of the underlying magnetic rocks.

In contrast, the EBS and WBS present lower magnetic anomalies primarily due to their composition of younger sedimentary rocks with reduced magnetic susceptibility compared to the older rocks found in the basin boundaries and the Shatsky Ridge. Furthermore, the presence of a thick sedimentary layer covering the EBS and WBS masks the magnetic basement rocks, leading to a diminished magnetic anomaly.

The Shatsky Swell consists of the Gudanta and Ochamchiri domes, which are aligned with the structural features of the Dzirula Massif in Georgia and are composed of Cretaceous and Jurassic rock sequences. A significant positive magnetic anomaly of approximately 300 nT is depicted in Figure 4, possibly attributable to the presence of volcanic rocks. This observation implies the potential extension of Middle Jurassic volcanics, particularly Bajocian volcanics originating from the Dzirula Massif and the Gagro-Chjawa zone of the southern slope of the Greater Caucasus, into the Shatsky Swell. The Shatsky Swell

is viewed as a connecting region between the areas featuring Jurassic volcanics in the Caucasus and the Crimea Highland. In addition, the analysis of magnetic data reveals a correlation between the magnetic anomalies observed in the Pontides region and the occurrence of Cretaceous-Eocene volcanic rocks, which are extensively documented along the entire coastline. This distinctive feature is characterized by prominently positive magnetic anomalies in the northern part of Türkiye's shoreline.

Edge detection techniques, namely the tilt angle and local wavenumber (LW), were utilized to enhance the interpretation of the magnetic data, as illustrated in Figure 5. The adoption of the tilt angle method was deemed appropriate due to its effectiveness in improving the interpretation of the signal field, which spans a range of ± 1.57 radians. This particular technique proves valuable in accentuating weaker anomalies while equalizing stronger ones, enabling the identification of subtle magnetic anomalies. It is important to note that the sign of the tilt angle is determined by the vertical derivative, as the total horizontal derivative consistently maintains a positive value. Consequently, a direct comparison between the vertical derivative and the total horizontal derivative can be made, further aiding the interpretation process.

The LW technique is used for a variety of reasons. The first reason is that because of it uses second derivatives of the magnetic potential and its capacity to highlight magnetic anomalies with short wavelengths, it is a valuable tool in the analysis of shallower tectonic structures. Secondly, LW map presents higher resolution over the contacts especially narrower structures such as dykes. Finally, the depth of the contact can be estimated by inverse of the local maxima values of the LW (Fairhead, 2016).

The tilt angle map presented in Figure 5a reveals negative readings within the basin and positive values over the ridges and basin boundary. The sign of the tilt angle is influenced by the distribution and orientation of magnetic rocks. Horizontally stratified magnetic rocks within the EBS and WBS contribute to elevated values in the horizontal magnetic field and reduced values in the vertical derivative. Additionally, the presence of younger sedimentary rocks in the basin,

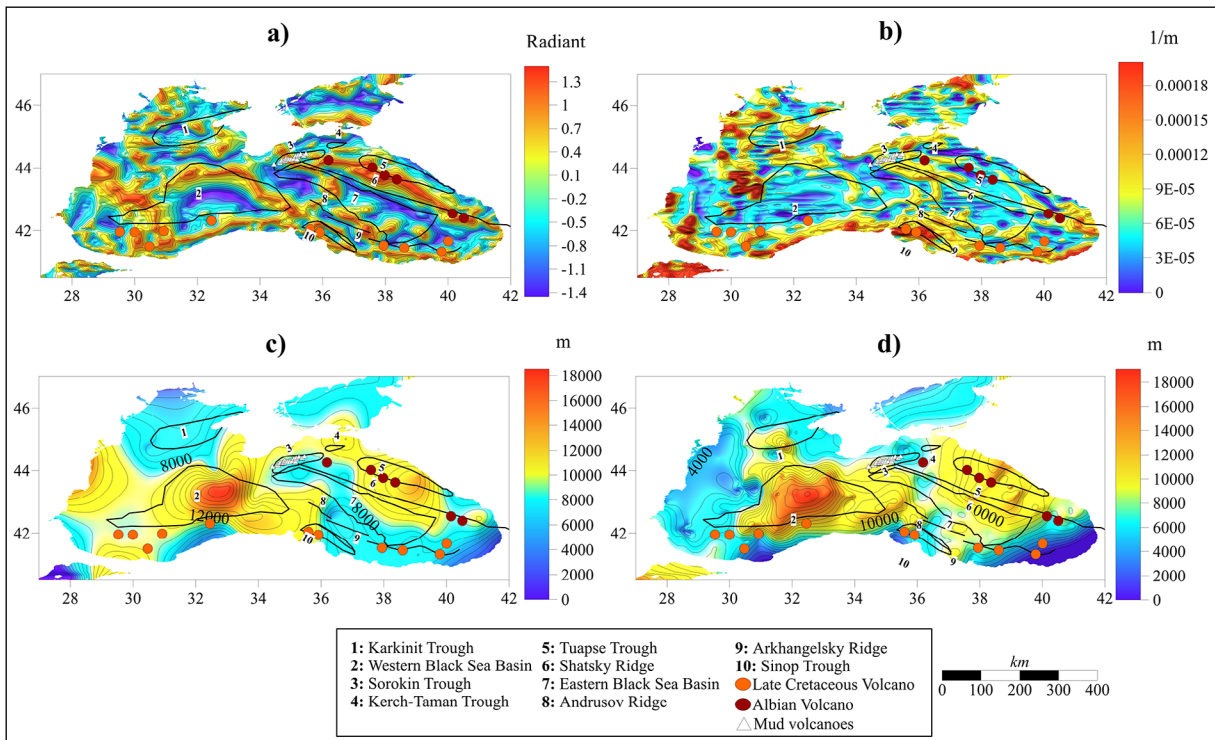


Figure 5- Results of the edge detection methods with tectonic features in the study area: a) Tilt angle map, b) LW map, c) tilt depth, d) LW depth.

exhibiting a negative magnetic susceptibility, results in notable negative anomalies within the tilt angle map. In contrast, ridges often consist of vertically-oriented magnetic rocks, which yield higher values in the vertical derivative and positive tilt angle values. These rocks exhibit a positive magnetic susceptibility. Thus, the determination of the tilt angle map's sign hinges upon the arrangement and quantity of magnetic rocks. At the interface between basement and sedimentary rocks, a sudden shift in magnetic characteristics occurs, leading to an immediate change in the magnetic field and a steep gradient along the edges. Nonetheless, this gradient approaches zero at two neighboring points along the contact boundary. Consequently, tilt angle values either become zero or converge to zero at contact points between distinct rock units.

The LW map, obtained by computing the first and second derivatives of the magnetic field, exhibits local maxima at the contacts between distinct rock types, as demonstrated in Figure 5b. These contacts represent locations where substantial variations in magnetic properties occur, resulting in prominent gradients

that can be detected through the first and second derivatives of the magnetic field. The first derivatives, both in the horizontal and vertical directions, enable the detection of the magnetic field's rate of change, while the second derivatives, also in the horizontal and vertical directions, are particularly responsive to abrupt changes within the LW map. Thus, the presence of local maxima within the LW map serves as a reliable indicator of the existence of notable magnetic gradients.

Figure 5c and 5d provide visual representations of the estimated depth of the uppermost portion of the contact, as inferred from the analysis of the tilt angle and LW maps. Notably, an overestimation of depth by approximately 18 km is observed in the WBS when compared to the EBS. This disparity can be attributed to a combination of factors, including tectonic structures, magmatic content, and sediment thickness.

One factor contributing to the exaggerated depth estimations in the WBS, as opposed to the EBS, is the presence of the Shatsky and Andrusov Ridges. Surrounding the EBS, these ridges generate shorter-

wavelength anomalies, resulting in shallower depth estimations derived from both the tilt depth and LW depth analyses.

Another influential factor is the magma content of the EBS and WBS. The WBS is characterized as magma-poor, while the EBS is known for its magma-rich nature (Kaymakçı et al., 2015). This discrepancy in magma composition directly affects the magnetic properties of the rocks and sediments within these basins, consequently influencing the resulting depth estimations.

Furthermore, sediment thickness plays a crucial role in the wavelength content of the tilt and LW maps. Typically, the WBS exhibits a higher sediment thickness compared to the EBS, leading to the observed overestimation of depth within the WBS.

In addition to employing edge detection methods, such as tilt and LW, the study area involved the calculation of Curie point depth (CPD) and heat flow. The CPD calculations were conducted by dividing

the study area into 65 blocks measuring 200×200 km each, with a 50% overlap between adjacent blocks. The size of these blocks played a crucial role in determining the vertical resolution of Z_b . Following the recommendation of Salem et al. (2014), a block size six times larger than the desired depth was utilized. In this particular study, a block size of 200×200 km resulted in an approximate vertical resolution of 33 km. The CPD values obtained were subsequently employed to infer the heat flow, disregarding the contribution of radiogenic heat production. Consequently, an inverse correlation is observed between the distribution of CPD and heat flow. The outcomes of the CPD calculations, top depth of the magnetic source derived from spectral analysis, and heat flow assessments are visually presented in Figure 6.

Figure 6a provides data indicating a greater Curie point depth (CPD) in the WBS as opposed to the EBS. Furthermore, the CPD values in the EBS exhibit abrupt changes, while the WBS demonstrates a more consistent pattern. These variations can be attributed

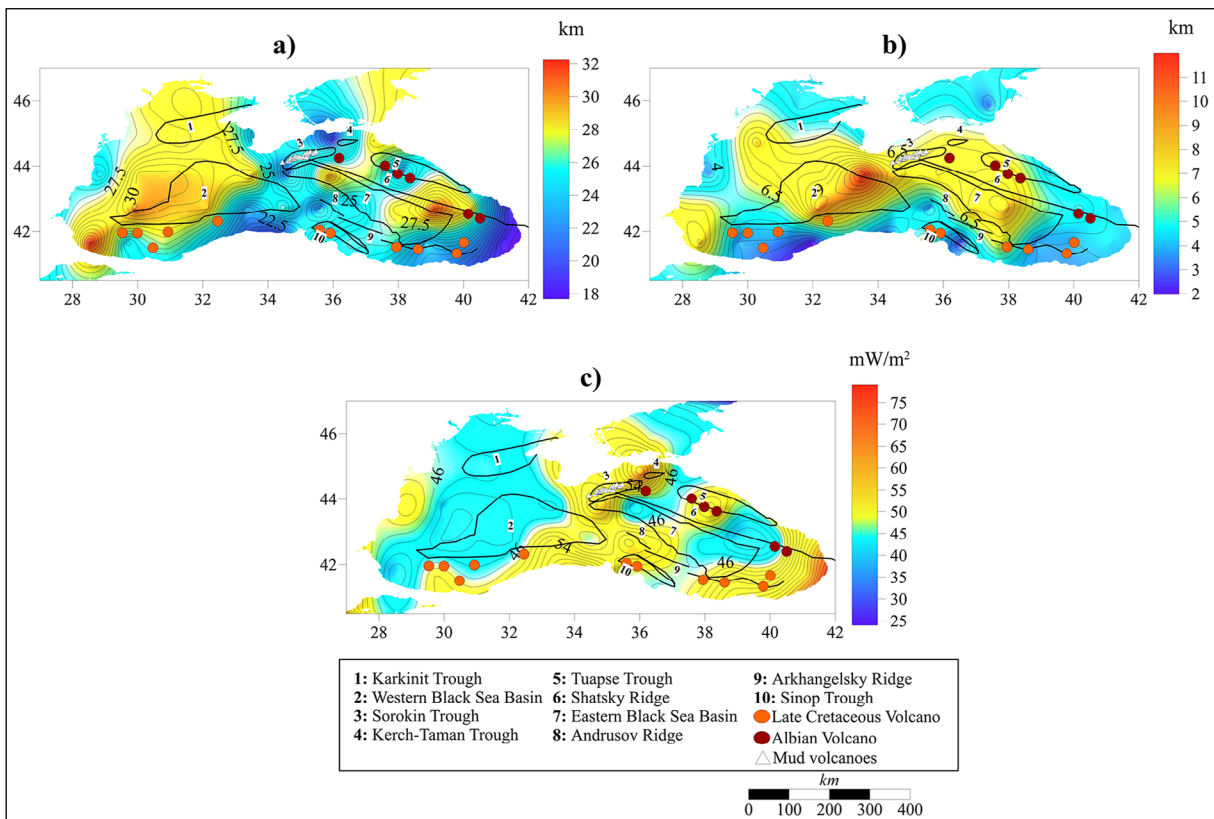


Figure 6- Results of the CPD, Z_i and heat flow with tectonic features in the study area: a) CPD map, b) Z_i map, c) heat flow map.

to various factors, including sediment thickness, the presence of volcanic rocks, and the tectonic history of the EBS and WBS.

To begin with, the thermal insulation provided by sediment thickness hinders heat transfer from the underlying mantle, resulting in deeper CPD values for both the EBS and WBS. Additionally, the WBS exhibits even deeper CPD readings in comparison to the EBS due to its thicker sediment cover.

Moreover, the presence of volcanic rocks enhances the amplitude of higher wavenumber sections, leading to shallower CPD values in the EBS. Furthermore, the abundance of volcanic rocks within the Shatsky Ridge, situated in the northeastern part of the Black Sea, influences the computation of CPD estimates in the EBS. The spectral characteristics of the short-wavelength magnetic anomaly originating from the Shatsky Ridge impact the CPD calculations in the adjacent blocks of the EBS, resulting in underestimated CPD values within the EBS.

Lastly, it is important to note the active tectonic processes occurring in the EBS, while the WBS exhibits a relatively more stable condition. The tectonic instability around the margins of EBS can trigger the upwelling of hot mantle materials. This explanation accounts for the shallower CPD values and higher heat flow observed in the EBS in comparison to the WBS. Letouzey et al. (1977) suggested that the higher heat flow values observed to the south of Crimea and west of the Caucasus might be associated with mud diapirism. Mud volcanoes are known to play a significant role in heat transfer, particularly in geothermal areas.

The Z_t map in Figure 6b provides insights into the top depth of the magnetic basement. Nevertheless, it is important to note that Z_t estimations are more subjective compared to the tilt and LW methods. Therefore, the Z_t estimations were solely utilized in correlation plots to facilitate a comparison of results with sediment thickness, LW maps, and tilt maps.

To facilitate additional investigation, two profiles were designated in the EBS and the WBS as illustrated in Figure 7. Profile A-A' was selected along the WBS, while profile B-B' was chosen along the EBS. These profiles were assessed to evaluate various parameters,

including global CPD (Li et al., 2017), Moho depth (Laske et al., 2013), estimated CPD values (Z_b values), LW depth, tilt depth, sediment thickness (Laske et al., 2013), Z_t values, and bathymetry data (Amante and Eakins, 2009).

The correlation plot depicted in Figure 8 was thoroughly examined to assess the relationships between different parameters along the A-A' and B-B' profiles. Based on the analysis, the following expected relationships between the parameters can be outlined:

- Moho depth and bathymetry are projected to exhibit an inverse correlation. This can be attributed to the requirement for the lithospheric load to be balanced or compensated by adjustments at the Moho interface, resulting in a reciprocal relationship between bathymetry and Moho depth.
- A positive correlation is anticipated between the estimated CPD and global CPD.
- A positive correlation is expected among LW depth, tilt depth, and Z_t values. These parameters provide valuable insights into the uppermost depth of the magnetic basement. Consequently, it is anticipated that at least two of these parameters will exhibit a positive correlation.
- The positive correlation between sediment thickness, LW depth, tilt depth, and Z_t values suggests a potentially rapid sediment accumulation process. The LW depth, tilt depth, and Z_t values are indicators of the top depth of the magnetic basement. If an increase in sediment thickness coincides with an increase in the top depth of the magnetic basement, it can be inferred that sedimentation accumulation rate remains unaffected by deformation, folding, seismic activity or variations in riverbed conditions.

The correlation plots shown in Figure 8 provide a quick and simultaneous comparison of various physical and geometric parameters. These correlation plots are essentially lower triangular matrices, where the comparison of the same geometric and physical parameters results in a value of 1.

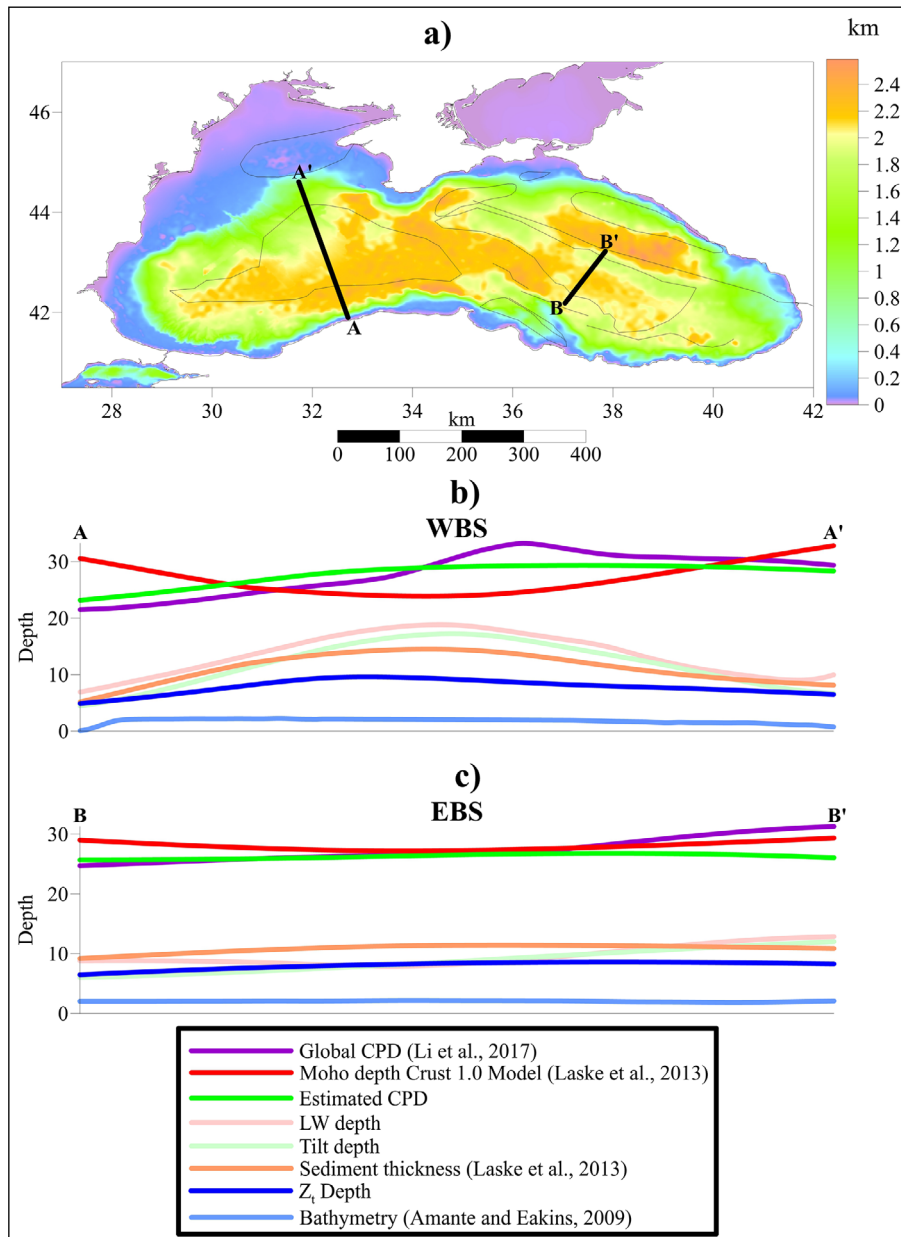


Figure 7- The selected profiles along the WBS and EBS: a) profile locations overlaid on the bathymetry, b) profile A-A' along the WBS, and c) profile B-B' along the EBS. Each profile includes the Global CDP, Moho depth, Estimated CDP, LW depth, Tilt Depth, sediment thickness, Z_i , and bathymetry.

Figure 8 presents the correlation analysis conducted for each variable along the A-A' profile representing the Western Black Sea (WBS) and the B-B' profile representing the EBS. The correlation coefficients range from -1 to 1, with 1 indicating a perfect positive correlation, 0 denoting no association, and -1 representing a complete inverse correlation. Specifically, the focus was on examining the correlation between the estimated Curie point depth (E CPD) and

the global CPD (G CPD) to compare our estimations with the findings reported by Li et al. (2017). Along the A-A' profile (WBS), a strong correlation of 0.93 is observed between G CPD and E CPD, while along the B-B' profile (EBS), a moderate correlation of 0.58 is found between these variables. It is anticipated to observe a high correlation between E CPD and G CPD. However, the relatively lower correlation along the B-B' profile may be attributed to various factors,

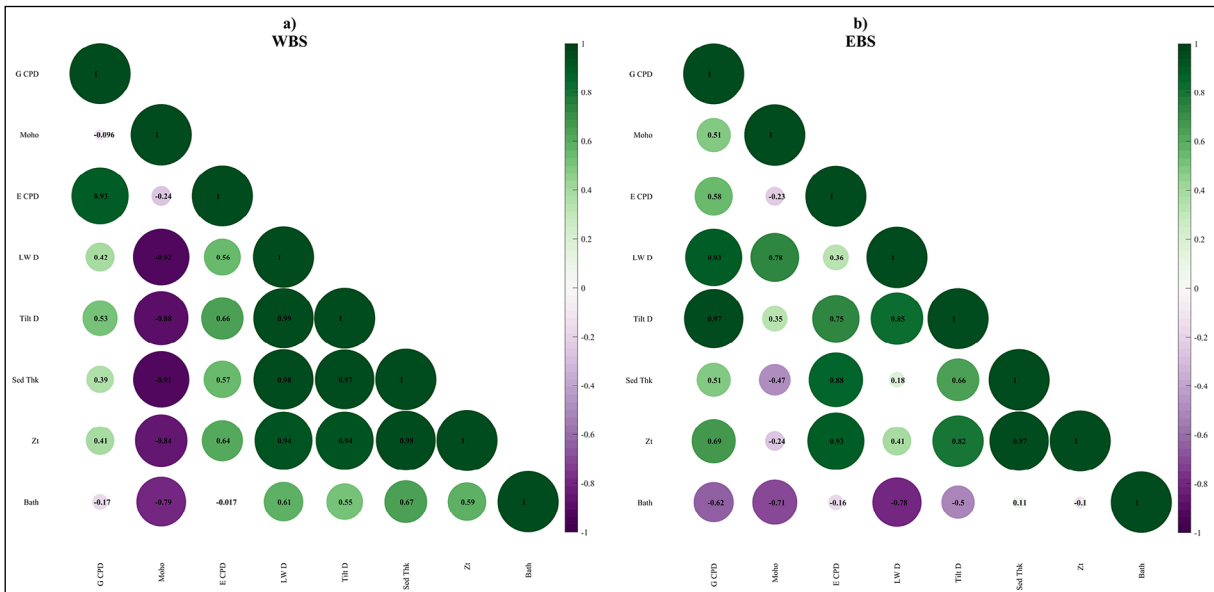


Figure 8- Correlation plots of WBS (A-A' profile) and EBS (B-B' profile). The radius of the circles is controlled by the correlation value. G CPD: global Curie point depth, Moho: Moho depth, E CPD: estimated Curie Point Depth, LW D: Local Wavenumber depth, Tilt D: Tilt depth, Sed Thk: sediment thickness, Z_t: top depth of the magnetic basement and Bath: bathymetry.

including the grid cell size, chosen block size, range of selected wavenumber components during CPD estimation, or the positioning of overlapping adjacent blocks.

As mentioned previously, Z_t, tilt depth (Tilt D), and LW depth (LW D) are indicators of the uppermost depth of the magnetic basement. Therefore, a strong correlation is expected among these variables, approaching a value of 1. Along the A-A' profile, the correlation between these variables exceeds 0.94, indicating a strong positive correlation. However, along the B-B' profile, while Tilt D - Z_t and Tilt D - LW D exhibit a high correlation, the correlation between LW D and Z_t is relatively low at 0.41. This lower correlation may arise from distinct characteristics of LW D and Z_t in the south-western part along the B-B' profile (Figure 7c).

The correlation between sediment thickness (Sed Thk), Tilt D, LW D, and Z_t plays a crucial role in understanding sediment accumulation rates. Along the A-A' profile, the correlation values between Sed Thk and LW D, Sed Thk and Tilt D, and Sed Thk and Z_t are above 0.97. These findings suggest a strong association between the top depth of the magnetic basement inferred by Tilt D, LW D, Z_t, and Sed Thk.

It is possible that the sediment deposition process remains uninterrupted by deformation, folding, seismic activity, or variations in riverbed conditions.

Furthermore, the higher sedimentation rate can be attributed to Balkanide Orogeny during Eocene. The Western Black Sea, being older, had more time for sediment deposition and provided a more suitable environment for sediment accumulation. Therefore, the expected outcome of a higher sediment accumulation rate in the WBS is justified by the correlation values of Sed Thk, Tilt D, LW D, and Z_t. Additionally, Nikishin et al. (2015) emphasized a higher sedimentation rate in the WBS from the Cretaceous to Eocene period, further supporting these findings.

The outcomes of Spadini et al. (1996) findings have yielded significant insights into the origins of the WBS and EBS regions, highlighting fundamental differences in their lithospheric properties. Notably, the WBS's formation can be attributed to the rifting of a thick lithosphere (approximately 200 km), characterised by lower temperatures and higher mechanical strength, thereby contributing to a substantial depth of necking (around 25 km). This thick lithosphere corresponds to the stable continental Moesian Platform. Conversely, the EBS's genesis is associated with the rifting of a

thinner lithosphere (approximately 80 km), resulting in elevated temperatures and weaker mechanical properties, leading to a shallower depth of necking (approximately 15 km). This scenario aligns well with the development of the EBS on the site of a prior (Mesozoic) back-arc basin (Spadini et al., 1996). To summarize, the geological history of the Black Sea region exhibits notable differences between its western and eastern basins. In the WBS, the rifting process was primarily responsible for the development of the stable Moesian Platform. On the other hand, in the Eastern Black Sea, a younger extensional basin was formed, overlaying a pre-existing area that had previously acted as a back-arc basin since the Early Jurassic period. This intriguing contrast in geological evolution sheds light on the diverse tectonic processes shaping the Black Sea basin's geology. These distinctive lithospheric properties and structural features offer plausible explanations for the observed variations in correlation plots between the Eastern and Western Black Sea regions.

6. Conclusion

This study presents a comprehensive theoretical framework aimed at unravelling the origin of the Black Sea, with a specific emphasis on both the East and West Black Sea basins. By leveraging a diverse range of data, including CPD values, heat flow values derived from CPD data, bathymetry, Moho depth, sediment thickness, and magnetic depth estimation techniques (Tilt angle and LW methods), a detailed examination of the region's geological characteristics has been conducted. Particularly, the impact of volcanic rock distribution on magnetic anomalies within the Black Sea area has been investigated. Moreover, an extensive analysis of the correlations between CPD values, bathymetry, Moho depth, sediment thickness, tilt depth, and LW depths was performed independently for the EBS and WBS basins. By scrutinizing these correlations in light of the tectonic history and presence of volcanic rocks, the significant disparities observed between the EBS and WBS have been thoroughly interpreted. This research has provided valuable insights into the distinct geological processes and contributing factors that have shaped the development and divergence of the EBS and WBS.

On the whole major findings in this study can be summarised as:

- Edge detection techniques, namely the tilt angle and LW methods, have played a crucial role in enhancing the interpretation of magnetic data. The analysis of tilt angle and LW maps reveals a significant difference in the estimated uppermost contact depth between the WBS and the EBS, with the WBS showing an approximately 18 km higher depth than the EBS.
- The WBS exhibits a higher Curie Point Depth (CPD), ranging up to 32 km, compared to the East Black Sea (EBS), where CPD values range between 24 to 28 km. Additionally, the CPD values in the EBS demonstrate abrupt changes, while the WBS displays a more consistent pattern, indicating the presence of thermal and magnetic property variations between these two regions.
- The correlation between Sed Thk, Tilt D, LW D, and Z_c is crucial for assessing sediment accumulation rates. Along the A-A' profile, the correlation values between these variables are all above 0.97, indicating a strong association between the top depth of the magnetic basement and sediment thickness. This suggests undisturbed sediment deposition, unaffected by deformation, folding, seismic activity, or variations in riverbed conditions.
- In aggregate, the findings derived from this empirical inquiry delineate that the two basins underwent divergent tectonic processes.

Acknowledgement

We would like to express our gratitude to National Centres for Environmental Information (NOAA) for EMAG2 and ETOPO1 data, and University of California San Diego (UCSD) for CRUST1.0 data.

References

- Akar, F. 2024. The upper crustal thermal structure of the Cameli Basin and its surroundings (SW Anatolia, Türkiye) by using the fractal-based centroid method of aeromagnetic data and its relationship with earthquakes occurring in the region. *Frontiers in Earth Science* 12, 1369742.

- Amante, C., Eakins, B. W. 2009. ETOPO1 1 Arc-Minute Global Relief Model: Procedures, Data Sources and Analysis. NOAA Tech. Memo. NOAA Technical Memorandum NESDIS NGDC-24.
- Audet, P., Gosselin, J. M. 2019. Curie depth estimation from magnetic anomaly data: A re-assessment using multitaper spectral analysis and Bayesian inference. *Geophysical Journal International*. 218, 494–507.
- Bhattacharyya, B. K., Leu, L. K. 1975. Analysis of magnetic anomalies over Yellowstone National Park: Mapping of Curie point isothermal surface for geothermal reconnaissance. *Journal of Geophysical Research*. Res. 80, 4461–4465.
- Bhattacharyya, B. K., Leu, L. K. 1977. Spectral analysis of gravity and magnetic anomalies due to rectangular prismatic bodies. *Geophysics* 42, 41–50.
- Bilim, F., Aydemir, A., Ateş, A., Dolmaz, M. N., Koşaroğlu, S., Erbek, E. 2021. Crustal thickness in the Black Sea and surrounding region, estimated from the gravity data. *Marine and Petroleum Geology*, 123, 104735.
- Bouguern, A., Allek, K., Khalifa, M., Bendiab, F., Boubaya, D. 2015. Mapping curie point depth of the west African Craton from satellite magnetic data and its implication for diamond exploration, in: *Proceedings of the 24th International Mining Congress of Turkey, IMCET 2015*, 351–359.
- Carrillo-de la Cruz, J. L., Prol-Ledesma, R. M., Velázquez-Sánchez, P., Gómez-Rodríguez, D. 2020. MAGCPD: A MATLAB-based GUI to calculate the Curie point-depth involving the spectral analysis of aeromagnetic data. *Earth Science Informatics*. 13, 1539–1550.
- Connard, G., Couch, R., Gemperle, M. 1983. Analysis of aeromagnetic measurements from the Cascade Range in central Oregon (geothermal resource area, USA). *Geophysics* 48, 376–390.
- Doğru, F., Pamukçu, O., Özsöz, I. 2017. Application of tilt angle method to the bouguer gravity data of Western Anatolia. *Bulletin of the Mineral Research and Exploration*. 155, 213–222.
- Dunlop, D., Özdemir, Ö., Fuller, M. D. 1998. *Rock Magnetism: Fundamentals and Frontiers*. *Physics Today*. 51, 64–66.
- Entezar-Saadat, V., Motavalli-Anbaran, S. H., Jamasb, A., Zeyen, H. 2020. A comprehensive lithospheric study of Black Sea using thermal modeling and simultaneous joint 3D inversion of potential field data. *Tectonophysics* 779, 228385.
- Espurt, N., Hippolyte, J. C., Kaymakçı, N., Sangu, E. 2014. Lithospheric structural control on inversion of the southern margin of the black sea basin, central pontides, Turkey. *Lithosphere* 6, 26–34.
- Fairhead, D. 2016. *Ebook: Advances in Gravity and Magnetic Processing and Interpretation*. Earthdoc.
- Finetti, I., Bricchi, G., Del Ben, A., Pipan, M., Xuan, Z. 1988. Geophysical study of the Black Sea, *Bollettino di Geofisica Teorica ed Applicata* 30(117-118), 197-324.
- Fourier, J. B. J. 1878. The analytical theory of heat. <https://doi.org/10.1017/CBO9780511693205>
- Gasparini, P., Mantovani, M. S. M., Corrado, G. and Rapolla, A. 1979. Depth of Curie temperature in continental shields: a compositional boundary?. *Nature*, 278(5707), 845-846.
- Görür, N. 1988. Timing of opening of the Black Sea basin. *Tectonophysics* 147, 247–262.
- Görür, N., Tüysüz, O., Aykol, A., Sakınç, M., Yigitbaş, E., Akkok, R. 1993. Cretaceous red pelagic carbonates of northern Turkey: their place in the opening history of the Black Sea. *Eclogae Geologicae Helveticae*. 86, 819–838.
- Haggerty, S. E. 1978. Mineralogical constraints on Curie isotherms in deep crustal magnetic anomalies. *Geophysical Research Letters*. 5, 105–108.
- Hippolyte, J. C., Müller, C., Sangu, E., Kaymakçı, N. 2017. Stratigraphic comparisons along the Pontides (Turkey) based on new nannoplankton age determinations in the Eastern Pontides: Geodynamic implications. *The Geological Society Special Publications*. 428, 323–358.
- Hippolyte, J. C., Murovskaya, A., Volfman, Y., Yegorova, T., Gintov, O., Kaymakçı, N., Sangu, E. 2018. Age and geodynamic evolution of the Black Sea Basin: Tectonic evidences of rifting in Crimea. *Marine and Petroleum Geology*. 93, 298–314.
- Kaymakçı, N., Graham, R., Horn, W. H. 2015. Geology and tectonics of Black Sea basin based on deep seismic reflection data, 68th Geological Congress of Turkey, 28–29.
- Laske, G., Masters, G., Ma, Z., Pasyanos, M. 2013. Update on CRUST1. 0—A 1-degree global model of Earth's crust, *Geophysical Research Abstracts* 15(15), 2658.
- Letouzey, J., Duval, B., Dorkel, A., Gonnard, R., Kristchev, K., Montadert, L. 1977. *The black-sea: a marginal basin geophysical and geological data, Structural History of the Mediterranean Basins*, 363–76. Paris.
- Li, C. F., Lu, Y., Wang, J. 2017. A global reference model of Curie-point depths based on EMAG2. *Scientific Reports*. 7.

- Maden, N. 2013. Geothermal structure of the eastern Black Sea basin and the eastern Pontides orogenic belt: Implications for subduction polarity of Tethys oceanic lithosphere. *Geology Frontiers*. 4, 389–398.
- Martos, Y. M., Catalán, M., Galindo-Zaldívar, J. 2019. Curie Depth, Heat Flux, and Thermal Subsidence Reveal the Pacific Mantle Outflow Through the Scotia Sea. *Journal of Geophysical Research: Solid Earth*. 124, 10735–10751.
- Martos, Y. M., Catalán, M., Jordan, T.A., Golynsky, A., Golynsky, D., Eagles, G., Vaughan, D. G. 2017. Heat Flux Distribution of Antarctica Unveiled. *Geophysical Research Letters*. 44, 11,417-11,426.
- Maus, S., Barckhausen, U., Berkenbosch, H., Bournas, N., Brozena, J., Childers, V., Dostaler, F., Fairhead, J. D., Finn, C., Von Frese, R. R. B., Gaina, C., Golynsky, S., Kucks, R., Lühr, H., Milligan, P., Mogren, S., Müller, R.D., Olesen, O., Pilkington, M., Saltus, R., Schreckenberger, B., Thébaud, E., Tontini, F. C. 2009. EMAG2: A 2-arc min resolution Earth Magnetic Anomaly Grid compiled from satellite, airborne, and marine magnetic measurements. *Geochemistry, Geophysics Geosystems* 10.
- Miller, H. G., Singh, V. 1994. Potential field tilt-a new concept for location of potential field sources. *Journal of Applied Geophysics*. 32, 213–217.
- Neprochnov, Y. P., Ross, D. A. 1978. Black Sea Geophysical Framework, in: Initial Reports of the Deep Sea Drilling Project, 42 Pt. 2. U.S. Government Printing Office.
- Nikishin, A. M., Korotaev, M. V., Ershov, A. V., Brunet, M. F. 2003. The Black Sea basin: tectonic history and Neogene–Quaternary rapid subsidence modelling. *Sedimentary Geology*, 156, 149–168.
- Nikishin, A.M., Okay, A. I., Tüysüz, O., Demirer, A., Amelin, N., Petrov, E. 2015. The Black Sea basins structure and history: New model based on new deep penetration regional seismic data. Part 1: Basins structure and fill. *Marine and Petroleum Geology*. 59, 638–655.
- Núñez Demarco, P., Prezzi, C., Sánchez Bettucci, L. 2021. Review of Curie point depth determination through different spectral methods applied to magnetic data. *Geophysical Journal International*, 224, 17–39.
- Okay, A.I. 1989. Tectonic Units and Sutures in the Pontides, Northern Turkey. *Tectonic Evolution of the Tethyan Region*. 109–116.
- Okay, A. I., Şengör, A. M. C., Görür, N. 1994. Kinematic history of the opening of the Black Sea and its effect on the surrounding regions. *Geology*, 22(3), pp.267-270.
- Okay, A. I., Şahintürk, O. 1997. AAPG Memoir 68: Regional and Petroleum Geology of the Black Sea and Surrounding Region. Chapter 15: Geology of the Eastern Pontides.
- Okay, A. I., Tüysüz, O. 1999. Tethyan sutures of northern Turkey. *Geological Society Special Publications*. 156, 475–515.
- Okubo, Y., Graf, R. J., Hansen, R. O., Ogawa, K., Tsu, H. 1985. Curie point depths of the Island of Kyushu and surrounding areas, Japan. *Geophysics* 50, 481–494.
- Özsöz, İ. 2021. Combined qualitative and quantitative regional interpretation of the thermal results of magnetic data in the eastern mediterranean region. *Turkish Journal of Earth Sciences*. 30, 665–680.
- Özsöz, İ. Toker, C. E. 2022. Interpretation of satellite gravity anomalies with pseudo-depth slicing method filter in Turkey. *Bulletin of the Mineral Research and Exploration*. 1–39.
- Pamuk, E., Özsöz, İ. 2022. Estimation of Curie-Point Depths and Heat Flow from Spectral Analysis of EMAG2 Magnetic Data in Cyprus Island. *Annals of Geophysics*. 65.
- Pasyanos, M. E., Masters, G., Laske, G., Ma, Z., Agu, S., Francisco, C., Artemieva, I. M., Mooney, W. D., Bassin, C. 2013. LITHO1.0-An Updated Crust and Lithospheric Model of the Earth Developed Using Multiple Data Constraints, *Geophysical Research Abstracts*.
- Phillips, J. D. 2000. Locating magnetic contacts: A comparison of the horizontal gradient, analytic signal, and local wavenumber methods. *SEG Technical Program Expanded Abstracts*. 19, 402–405.
- Ravat, D., Morgan, P., Lowry, A. R. 2016. Geotherms from the temperature-depth-constrained solutions of 1-D steady-state heat-flow equation. *Geosphere* 12, 1187–1197.
- Robinson, A., Spadini, G., Cloetingh, S., Rudat, J. 1995. Stratigraphic evolution of the Black Sea: inferences from basin modelling. *Marine and Petroleum Geology*. 12, 821–835.
- Robinson, A. G., Rudat, J. H., Banks, C. J., Wiles, R. L. F. 1996. Petroleum geology of the Black Sea. *Marine and Petroleum Geology*. 13, 195–223.
- Ross, H. E., Blakely, R. J., Zoback, M. D. 2006. Testing the use of aeromagnetic data for the determination of Curie depth in California. *Geophysics* 71.
- Rozimant, K., Büyüksaraç, A., Bektaş, Ö. 2009. Interpretation of magnetic anomalies and estimation of depth

- of magnetic crust in Slovakia. *Pure and Applied Geophysics* 166, 471-484.
- Salem, A., Green, C., Ravat, D., Singh, K.H., East, P., Fairhead, J.D., Mogren, S., Biegert, E. 2014. Depth to Curie temperature across the central Red Sea from magnetic data using the de-fractal method. *Tectonophysics* 624–625, 75–86.
- Salem, A., Williams, S., Fairhead, J. D., Ravat, D., Smith, R. 2007. Tilt-depth method: A simple depth estimation method using first-order magnetic derivatives. *The Leading Edge*. 26, 1502–1505.
- Şengör, A. M. C. 1984. The cimmeride orogenic system and the tectonics of Eurasia. *Spec. Pap. Geol. Soc. Am.* 195, 1–74.
- Shillington, D. J., Scott, C. L., Minshull, T. A., Edwards, R. A., Brown, P. J., White, N. 2009. Abrupt transition from magma-starved to magma-rich rifting in the eastern Black Sea. *Geology* 37, 7–10.
- Sobh, M., Gerhards, C., Fadel, I., Götze, H. J. 2021. Mapping the Thermal Structure of Southern Africa From Curie Depth Estimates Based on Wavelet Analysis of Magnetic Data With Uncertainties. *Geochemistry, Geophysics, Geosystems* 22.
- Spadini, G., Robinson, A., Cloetingh, S. 1996. Western versus Eastern Black Sea tectonic evolution: Pre-rift lithospheric controls on basin formation. *Tectonophysics* 266, 139–154.
- Spector, A., Grant, F.S. 1970. Statistical models for interpreting aeromagnetic data. *Geophysics* 35, 293–302.
- Starostenko, V. I., Dolmaz, M. N., Kutas, R. I., Rusakov, O. M., Oksum, E., Hisarlı, Z. M., Okyar, M., Kalyoncuoğlu, U. Y., Tütünsatar, H. E., Legostaeva, O. V. 2014. Thermal structure of the crust in the Black Sea: comparative analysis of magnetic and heat flow data. *Marine Geophysical Research*. 35, 345–359.
- Tanaka, A., Okubo, Y., Matsubayashi, O. 1999. Curie point depth based on spectrum analysis of the magnetic anomaly data in East and Southeast Asia. *Tectonophysics* 306, 461–470.
- Tari, E., Şahin, M., Barka, A., Reilinger, R., King, R.W., McClusky, S., Prilepin, M. 2000. Active tectonics of the Black Sea with GPS. *Earth, Planets and Space*. 52, 747–751.
- Tari, G. C., Simmons, M. D. 2018. History of deepwater exploration in the Black Sea and an overview of deepwater petroleum play types. *Geological Society Special Publications*. 464, 439–475.
- Thurston, J. B., Smith, R. S. 1997. Automatic conversion of magnetic data to depth, dip, and susceptibility contrast using the SPI (TM) method. *Geophysics* 62, 807–813.
- Tütünsatar, H. E., Dolmaz, M. N., Oksum, E., Okyar, M., Kalyoncuoğlu, U. Y., Starostenko, V., Kurtas, R.I., Rusakov, O., Legostaeva, O., Hisarlı, Z. M. 2018. The Relation between Heat Flow Obtained by Curie Depth Point (CDP) and the Faults and Gas Leaks in the Black Sea. *Physics and Astronomy International Journal*. 2, 65–68.
- Tüysüz, O. 2018. Cretaceous geological evolution of the Pontides. *Geological Society Special Publications*. 464, 69–94.
- Tüysüz, O., Yılmaz, I. Ö., Švábenická, L., Kirici, S. 2012. The unaz formation: A key unit in the western black sea region, N Turkey. *Turkish Journal of Earth Sciences*. 21, 1009–1028.
- Verduzco, B., Fairhead, J. D., Green, C. M., MacKenzie, C. 2004. New insights into magnetic derivatives for structural mapping. *Lead. Edge (Tulsa, OK)* 23, 116–119.
- Wagner-Friedrichs, M., Krastel, S., Spiess, V., Ivanov, M., Bohrmann, G., Meisner, L. 2008. Three-dimensional seismic investigations of the Sevastopol mud volcano in correlation to gas/fluid migration pathways and indications for gas hydrate occurrences in the Sorokin Trough (Black Sea). *Geochemistry, Geophysics Geosystems* 9.
- Zonenshain, L. P., Le Pichon, X. 1986. Deep basins of the Black Sea and Caspian Sea as remnants of Mesozoic back-arc basins, *Tectonophysics* 123(1-4), 181-211.